Pore-scale studies of spontaneous imbibition into oil-saturated porous media

Can Ulas Hatiboglu and Tayfun Babadagli*

Department of Civil and Environmental Engineering, School of Mining and Petroleum, University of Alberta, 3-112 Markin CNRL-NREF, Edmonton, AB, Canada T6G 2W2

(Received 27 November 2007; revised manuscript received 6 May 2008; published 27 June 2008)

Spontaneous imbibition phenomenon was modeled using the lattice Boltzmann method (LBM). The model was validated using silicon-etched micromodel and sandpack visualization experiments. The strongly water-wet model saturated with oil (kerosene or mineral oil) was exposed to distilled water in order for a capillary interaction to take place under static conditions. These experiments mimic the transfer between rock matrix and fracture during any wetting phase flow in fractures while the matrix contains a nonwetting phase as encountered in oil, gas, and geothermal reservoirs as well as during the application of subsurface CO_2 sequestration or waste disposal reservoirs. Despite the vast amount of research work on this common process, pore-scale investigations and modeling are limited especially at small time scales. The results showed that the LBM captures the physics of the process at pore scale for low viscosity values of nonwetting phase for any type of (cocurrent or countercurrent imbibition) interaction.

DOI: 10.1103/PhysRevE.77.066311 PACS number(s): 47.56.+r, 47.55.nb, 05.50.+q

I. INTRODUCTION

Matrix-fracture interaction by spontaneous imbibition is a common process in production of oil, natural gas, and geothermal fluids from naturally fractured reservoirs and in environmental applications such as waste disposal, groundwater contamination, and subsurface sequestration of greenhouse gases. It also finds a vast amount of applications in the surface chemistry related industry. Many different aspects of the process were studied using continuum or stochastic models for mainly practical purposes over the last four decades. Understanding the physics of the process at pore scale requires more experimental research and robust modeling techniques to capture the physics of the process for especially unfavorable rock and fluid characteristics for capillary interaction. In addition to this, it is important to define the process at the small time scale (second and/or minute level) to clarify the progress of the displacement of the nonwetting phase by the wetting phase and the development of residual oil saturation when the process is totally controlled by capillary forces.

Earlier studies mainly aimed to explain oil recovery by capillary imbibition in naturally fractured reservoirs [1–4]. Other works published later attempted to explain different aspects of the process such as matrix shape factor [5,6], wettability [7], and interfacial tension [8].

Recent attempts were mainly on understanding the physics of the process for challenging conditions. Hatiboglu and Babadagli [9,10] used core samples and sandpack models to describe matrix-fracture interaction under the influence of matrix shape, wettability, gravity, interfacial tension (IFT), oil viscosity, and rock type for cocurrent and countercurrent imbibition.

Advancements in technology allowed us to manufacture real-world sized silicon etched micromodels using sandstone thin section replicas. These models were used in pore scale capillary imbibition research very recently [11,12]. Imitating real core structure in real pore and grain sizes allowed exploring the fluid flow in pore size scale.

For the modeling part of this study, the lattice Boltzmann method (LBM) was utilized. It is relatively a new method with significant potential to simulate multiphase fluid flows. The model is under intense research in various disciplines, but its current form need improvements for modeling the transport process in porous media. The model simulates the flow through a particle transport approach, using simple rules for collisions, streaming, surface interactions avoiding complex mathematical equations. The LBM evolved from the lattice gas methods [13] which track individual particles and their interactions are typically limited to two-dimensional hexagonal grids. The LBM use near continuous particle distributions to avoid statistical noise associated with individual particles.

Pioneers of the method published numerous valuable resources [14–17]. In the present study, one of the three most popular methods (pseudopotential method), widely known as the Shan-Chen model, was used [18]. In our previous attempt, we adapted this method to model miscible interaction of two mixing phases (oil and solvent) [19]. The present study uses the same model for immiscible interaction of two phase separating fluids (oil and water) with some modifications. This was accomplished by the inclusion of fluid-fluid cohesion (interfacial tension) and fluid-solid adhesion (wettability) forces into the model. This transformation makes the LBM a very convenient algorithm to model immiscible fluid flow.

The Shan-Chen model is not based on thermodynamical principles, therefore, the interfacial tension and wettability is introduced empirically. The free-energy approach [20], on the other hand, implements interfacial thermodynamics, and therefore allows viscosity and interfacial tension to be specified *a priori*. Despite these advantages over the pseudopotential model, the free-energy model is computationally more demanding and has certain drawbacks [21,22].

Studies related to porous media among others include investigations of fluid interface configurations [23], capillary

*Corresponding author; tayfun@ualberta.ca

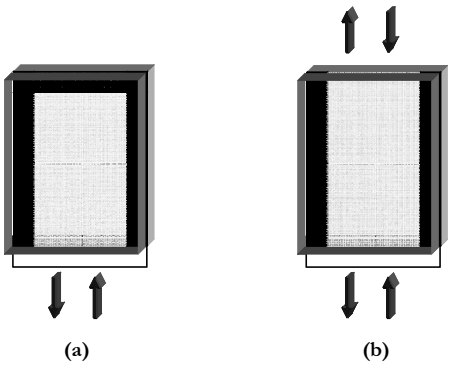

FIG. 1. Schematic representation of the experimental model with different boundary conditions: (a) countercurrent, and (b) cocurrent interaction.

rise [24], and solute transport [25]. Several investigations included qualitative comparisons between LBM simulation results and experimental data, but quantitative comparisons are less common.

Scaling or model parameter calibration arises as a critical issue in LBM development. Christensen [26] successfully calibrated the LBM for his needs. However the relation between physical and lattice time (which involves viscosity) is largely ignored due to the assumption that viscous forces are negligible compared to capillary forces.

In this study, both cocurrent and countercurrent spontaneous imbibition transfer process between matrix and fracture was modeled using the LBM for static condition. Two-dimensional (2D) sandpack and micromodel experiments were conducted to clarify the physics of the process at pore scale and to provide experimental support to validate the LBM model.

II. EXPERIMENTAL STUDY

Glass bead packed and silicon etched glass micromodels were used to obtain images of the spontaneous imbibition process at two different scales. For the larger glass bead packed models, transparent acrylic was chosen as enclosure material. The model is square in shape with the dimensions of 5×5 cm. To create porous medium, glass beads with 0.1 mm diameter were chosen. The gap between the two layers of acrylic was measured to be 0.3 mm. The glass beads were packed densely and homogeneously with the help of a shaker. Filter paper on one end of the model was used for mechanically stabilizing the glass beads as well as ensuring a smooth edge for the imbibing phase to enter. The thickness of the model was kept minimal to ensure 2D behavior.

Epoxy was found to be the most appropriate material in creating boundary conditions because of its inert behavior to oil types. Three edges of the models were sealed with epoxy to ensure the fluid interaction occurs through only one side creating a countercurrent-type transfer [Fig. 1(a)]. Similarly, cocurrent models were obtained sealing only the two opposing sides [Fig. 1(b)]. The properties of the fluids used in the experiments are tabulated in Table I and the schematic representation of the experimental setup is shown in Fig. 2.

TABLE I. Fluid pairs used in experiments.

	Water	Kerosene	Mineral oil
Density (g/cc)	0.99	0.79	0.83
Viscosity (cp)	1	2.9	36.32
Interfacial tension (dyne/cm) *- with water -*		46.1	33.2
Bond number *-with water -*		2.52×10^{-4}	2.84×10^{-4}
Capillary number		9.0×10^{-6}	1.57×10^{-4}
Reynolds number		2.92×10^{-3}	2.7×10^{-4}

For the micromodel study, the silicon etched model was preferred over the glass-etched models because of a few limiting factors. For glass etching, acid has to be used, where the reaction kinetics of acid etching makes it necessary to enlarge the pore sizes of typical rocks by a factor of 5 to 50. For silicon etching, however, pores and throats are created photochemically, resulting in 1:1 replication of a sandstone texture. A detailed description of the fabrication and construction process of the models was reported in several studies [27–29]. The pattern (Fig. 3) captured from a real sandstone thin section is 500 μm in length is repeated 10 000 times to create a 5 cm^2 model. The properties of the micromodel are listed in Table II.

The model was transparent from one side only, and the ports for inlet and outlet were positioned on the opaque side. Acrylic was chosen as the model holder with four configurable ports (Fig. 4) as a flat and smooth surface was required. An additional port was used for vacuuming the micromodel so as to keep it stable and prevent the ports from leaking (Fig. 5). Avoiding rubber isolators ensures that the model is perfectly horizontal in orientation and thickness is the same throughout the model.

The micromodels were saturated with either kerosene or mineral oil by applying vacuum from the two inlet ports. At the same time, the oleic phase was injected from the remaining two ports. The saturation procedure was continued until roughly 100 pore volume oil was circulated. Then, water was injected through the fracture (from point 1 in Fig. 4) to fill the fracture. Attention was paid to perform the injection at a very low rate to fill the fracture with water so as to obtain a fracture-matrix interaction by only capillarity rather than viscous forces. The fracture was filled with water quickly because of its extremely bigger size (2000 μm) compared to the largest pore size (150 μm). Then, the interaction between

TABLE II. Micromodel properties.

Porosity	35%
Permeability	1 md
Pore Sizes	1–150 μm
Throats	0.5–10 μm
Etch Depth	15 to 35 μm
Fracture width	2000 μm

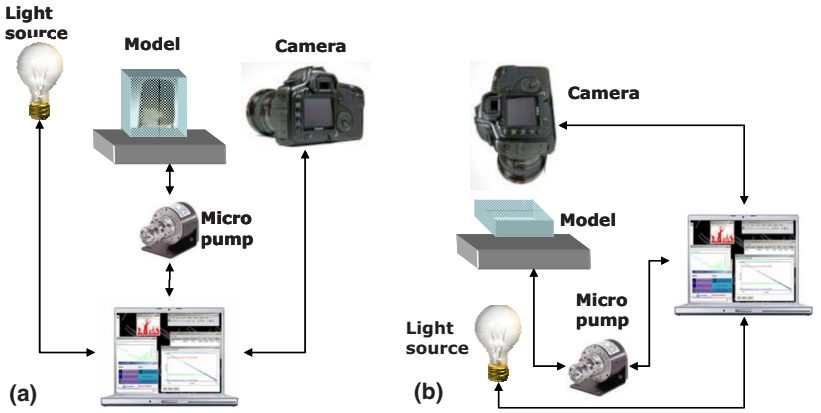

FIG. 2. (Color online) Experimental setup for (a) vertical, and (b) horizontal orientations.

the fluid filled in the fracture and oil in the matrix started as spontaneous imbibition. To keep enough amount of water in the fracture during the process, water injection was continued at a very slow rate as the injected fluid is produced from the production port located on the other end of fracture (Port No. 2 in Fig. 4).

A. Procedure

After constructing the glass bead models, they were saturated with the oleic phase; namely kerosene or mineral oil, under vacuum. Two different setups were used for vertical and horizontally oriented experiments (Fig. 2). In both experimental cases, a continuous supply of water was achieved using a micropump to feed the water container.

Light source is critical in obtaining good quality images. A high intensity halogen lamp was chosen to be appropriate. But this had to be cooled off properly not to affect the experimental results. To assure this, a fan cooled, computer controlled illumination system was constructed. The system made it possible to turn the light off, while not capturing the image, to prevent the excessive heat generation.

The visualization equipment consists of a 10 megapixel digital single-lens reflex camera, which was configured to perform time-lapse photography. A small piece of code was written to synchronize the light source and the camera.

An open source image processing software (ImageJ) was used for capturing and processing of the images because of its multi-image tiff file handling capability and ability to incorporate user written codes through plug-ins.

For the silicon etched micromodel, a Zeiss microscope with backlighting and a single-lens reflex (SLR) attachment was used. Since the light reflected from the model was minimal, long aperture times were required to be able to capture the image successfully. For that reason, it was required to use an SLR camera instead of a video camera. To minimize vibration, the setup was positioned on a vibration-free air table.

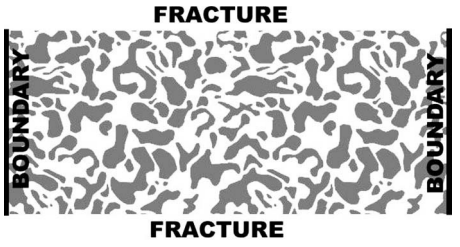

FIG. 3. Repetitive pattern (two patterns montaged side by side, fracture and boundaries are not to scale, fracture width: 2000 μm, average pore size: 75 μm).

B. Results

1. Glass bead models

Prior to saturation, depending on the desired interaction type, either three-sides-sealed (countercurrent) or two-sides-sealed (cocurrent) models were prepared. After populating the gap between the plexiglass sheets with glass beads homogeneously, the model was saturated with the oleic phase (mineral oil or kerosene) under vacuum. The final step was to position the sample in the water container to start the spontaneous imbibition.

2. Countercurrent interaction

In the countercurrent interaction of kerosene-water pairs for vertical positioning the fluid front progressed in a bulk fashion (Fig. 6). A systematic pattern was recognized with a stable front without any fingering.

The countercurrent interaction of the kerosene-water pairs was also conducted for horizontal displacement (Fig. 7) since the frontal displacement was suspected to be caused by sup-

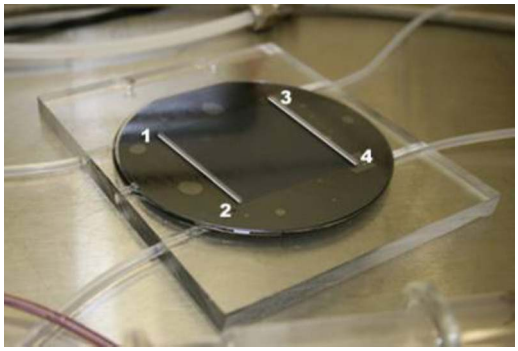

FIG. 4. (Color online) Glass model on holder, inlet-outlet ports connected, vacuum port disconnected. Ports on the model are marked with numbers, where port 1&2 and 3&4 are connected with fracture which is highlighted with gray lines.

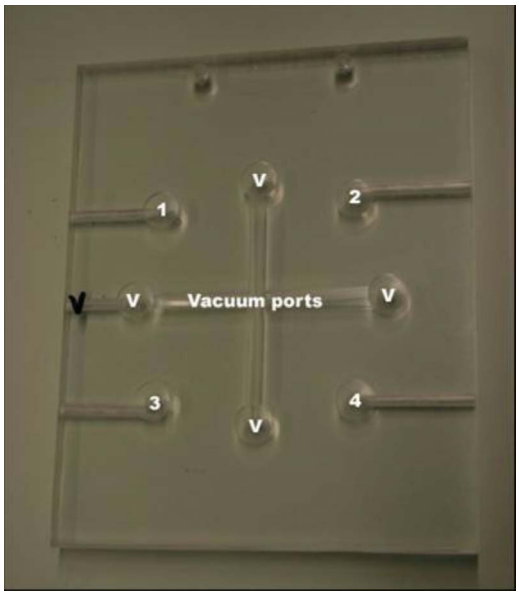

FIG. 5. (Color online) Model holder with four configurable ports and one vacuum port. Vacuum suction cups are connected to the vacuum port internally.

pressing gravity. Although the LBM matching was not performed due to observed viscosity limit in the stochastic modeling, as will be explained in the next section, the mineral oil equivalent of the same experiments was conducted and given in Fig. 8 as a reference. More random displacement was observed for both oil types unlike the vertical case. Capillary forces were totally dominating in this type of interaction. In the kerosene case, the sweep was inefficient initially where fingers did not grow in lateral direction but proceeded almost linearly until they reach the top boundary. Because of the viscosity difference, kerosene showed a faster displacement. For the mineral oil experiment, the situation was slightly different. The progress of the fluid front was suppressed because of oil viscosity. Hence, water tended to spread laterally developing an expanding branch pattern.

C. Cocurrent interaction

Cocurrent models are two-sides-sealed models and the experiments were performed under water contact from both bottom and top edges [Fig. 1(b)]. The effect of gravity was more apparent for these experiments for the mineral oil (Fig. 9), and kerosene (Fig. 10) samples.

In the mineral oil case (Fig. 9), one can see a massive fingering grown in downward direction caused by gravity. As the fluid front reaches down the bottom of the model, fingers started expanding laterally and this caused a slowdown of the spontaneous imbibition rate. Viscous fingering was expected to occur for the viscosity ratios of 10 cp and more. Thus no fingering is expected in the kerosene case having a viscosity ratio around 3 (Fig. 10). A good clean sweep because of the high mobility of kerosene can be observed.

D. Micromodel

For the micromodel study, silicon-etched micromodels were preferred, since they offered high accuracy in dimensions and perfect repeatability of the pattern. This would allow the LBM model to be tested precisely and accurately. This technique is also advantageous over conventional glass etching in preparing much smaller pore sizes, which is required in order for an effective spontaneous imbibition to take place.

Under the microscope, the progress of the fluid front was captured for the kerosene case (Fig. 11). The same experiment was repeated with the mineral oil and water pair (Fig. 12). One can observe the front progress and the development of residual oil saturation behind the front. Residual oil was observed to be strictly dependent on the pore and throat size and structure [Fig. 13(a)]. Note that the same experiment was repeated for mineral oil and it showed a very similar structure of residual oil saturation and front progress [Fig. 13(b)].

The velocity of the displacement front (ν) (to cover one repeated pattern length) was measured to be 500 μm/10 sec for both mineral oil and kerosene. To have an understanding of the fluid properties and porous media implications, dimensionless numbers were calculated (Table I). For the purpose of evaluating the effect of gravitational effects to capillary forces, the Bond number (B_o) [30] was calculated as

$$B_o = g(\rho_w - \rho_o)R/\sigma_{o-w}, \tag{1}$$

where R denotes the characteristic pore radius; for simplicity this is taken as 75 μm.

The capillary number (C_a) is calculated to investigate the ratio of viscous and capillary forces as

$$C_a = v^*\mu/(\theta^*\sigma_{o-w}), \tag{2}$$

where v denotes the fluid velocity and θ is porosity. The calculated numbers show that viscous forces are negligible compared to capillary forces for both oil types. The Reynolds number (R_e) would give further information by providing the ratio of inertial and viscous forces. Re is calculated as

$$\mathrm{Re} = \rho^* v^* R/\mu\theta. \tag{3}$$

Values are very small as expected and, therefore, these dimensionless quantities confirm that capillary forces dominate the system.

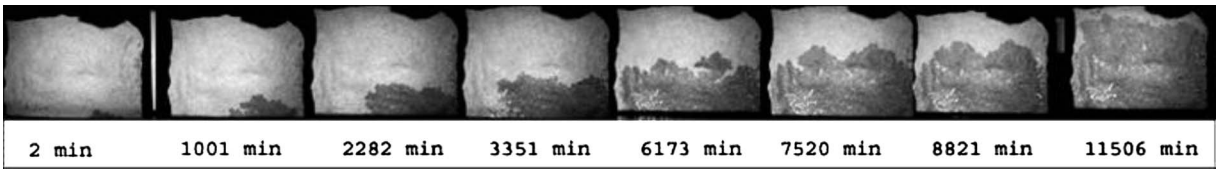

FIG. 6. Kerosene-water countercurrent imbibition on vertical orientation. Darker color represents the displacing-wetting-phase (water).

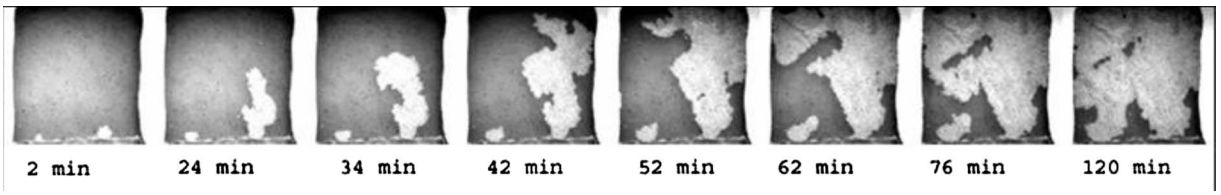

FIG. 7. Kerosene-water countercurrent imbibition (horizontal orientation). Lighter color represents the displacing-wetting-phase (water).

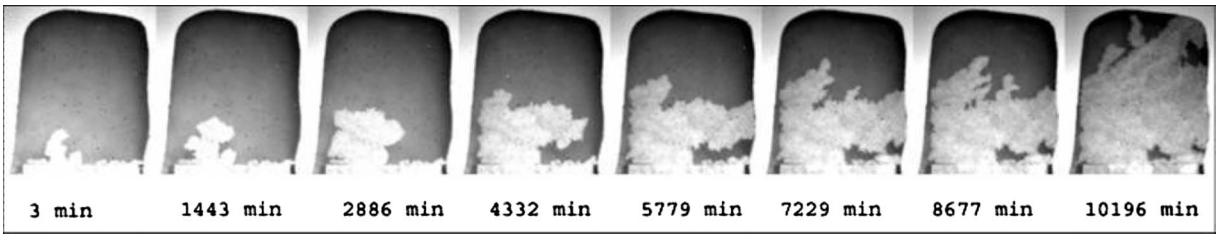

FIG. 8. Mineral-oil–water countercurrent spontaneous imbibition (horizontal orientation). Lighter color represents the displacing-wetting-phase (water).

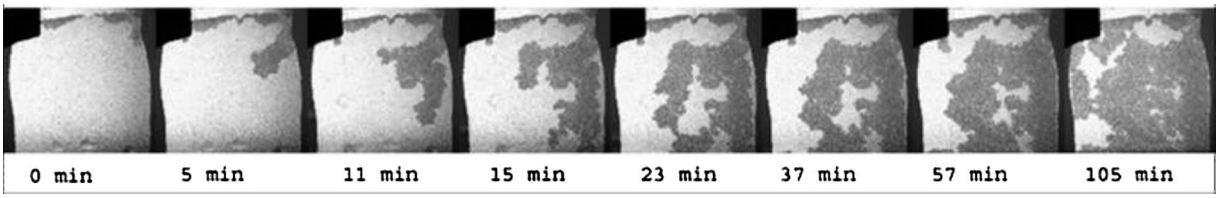

FIG. 9. Mineral-oil–water cocurrent spontaneous imbibition (vertical orientation). Darker color represents the displacing-wetting-phase (water).

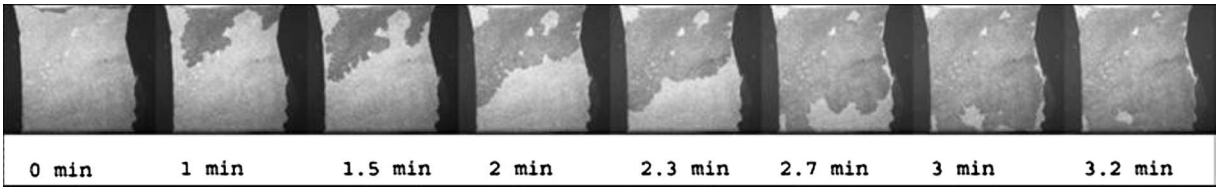

FIG. 10. Kerosene-water cocurrent imbibition (vertical orientation). Darker color represents the displacing-wetting-phase (water).

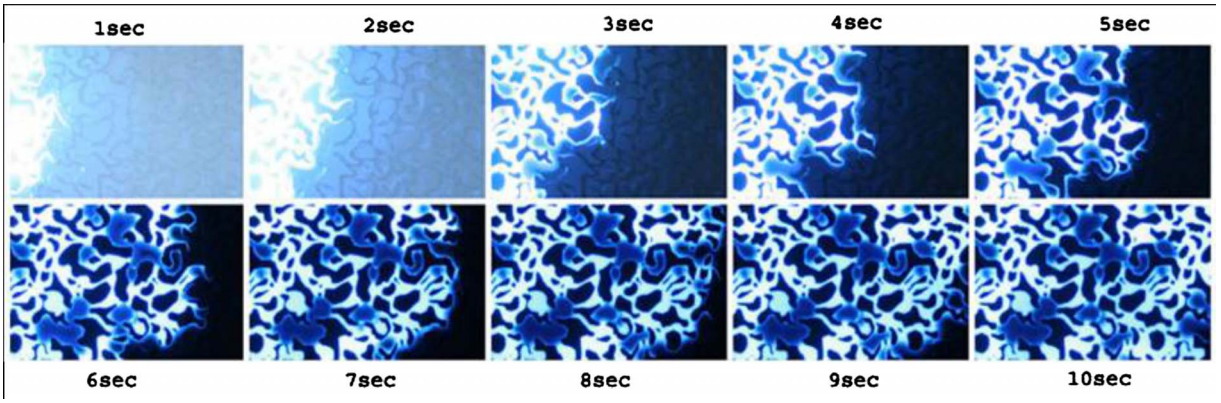

FIG. 11. (Color online) Time-lapse visualization of spontaneous imbibition on the micromodel. Water imbibes from left (white) displacing kerosene. The grains are in black color. Oil phase is in blue color (gray tones in the black and white print). Each image is 500 μm wide and magnified 20×.

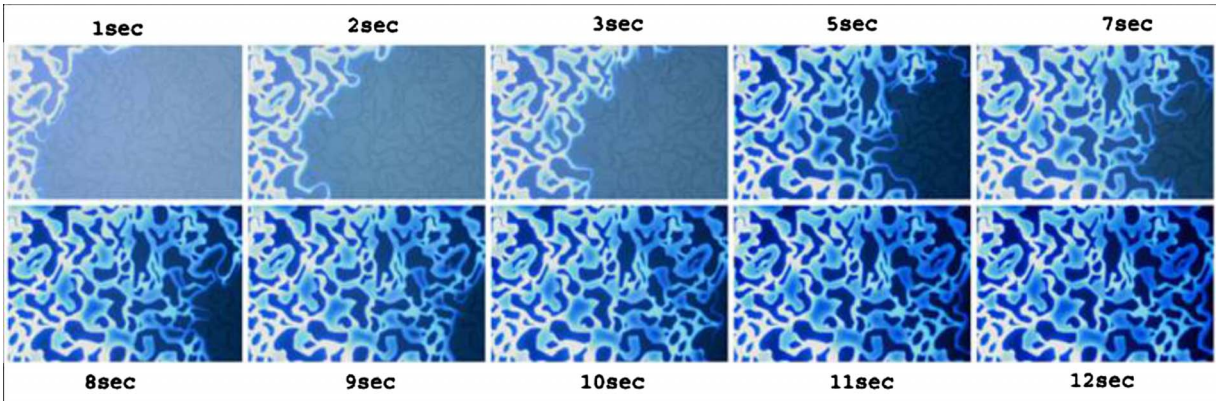

FIG. 12. (Color online) Visualization of spontaneous imbibition on the micromodel. Water imbibes from left (white) displacing mineral oil. The grains are in black color. Oil phase is in blue color (gray tones in the black and white print). Each image is 500 μm wide and magnified 20×.

III. MODELING–LATTICE-BOLTZMANN METHOD (LBM)

A. Model formulation

The LBM emerged from the lattice gas cellular automata (LGCA). The first generation of the model was not corresponding to the Navier-Stokes equation. It took quite a while to realize the importance of lattice symmetry [13]. Evolution continued by replacing the Boolean particle representations by particle distribution functions. Widely used Bhatnagar-Gross-Krook (BGK) approximation for the collision operator was introduced to the LBM by Qian *et al.* [31] and Chen *et al.* [32]. The abilities of the LBM attracted attention not only for its capability to simulate fluid flow through complex boundaries and interfacial dynamics, but also easily programmability for the parallel computers.

The model evolution was reviewed by several researchers [15–17]. Researchers dealt with immiscible processes [16,33,34,38], as well as miscible processes [35–37,39,40].

The proposed model, which was based on the pseudopotential method (widely known as the Shan-Chen model) [18], was previously used for another study conducted by the authors of this paper to model miscible interaction recently [19]. The method applied in the present study utilizes variables introduced by Shan and Chen [18] and Martys and Chen [38], respectively, to account for phase separation and wettability, with a newly introduced scaling strategy. For a detailed explanation of the algorithm, readers are referred to our previous study [19].

The LBM proposed in this study uses a nine-speed structure, in a square lattice which is commonly expressed as D2Q9 (two dimensions, nine velocities). The adapted Shan-Chen method (also known as pseudopotential) in which the basic variables of the models are the distribution functions, where R_i is red (water) and B_i is blue (oil) fluid densities. Shan and Chen introduced this model for immiscible displacement in porous media. We, in this study, adapted this model for spontaneous imbibition (quasistatic displacement) which requires a very low capillary number range.

R_i and B_i are the mean occupation numbers for red and blue fluid particles, respectively, in the direction i at a given node. The particles on each node have nine velocities (Fig. 14). The phases have identical collision equations with the only difference being the relaxation parameters for each phase which is depicted by the different viscosities of the fluids.

The formulation of the basic LBM algorithm that was summarized above can be found in the relevant publication [19]. This algorithm was not designed to handle external body forces, such as gravity, solid adhesion (wettability), or

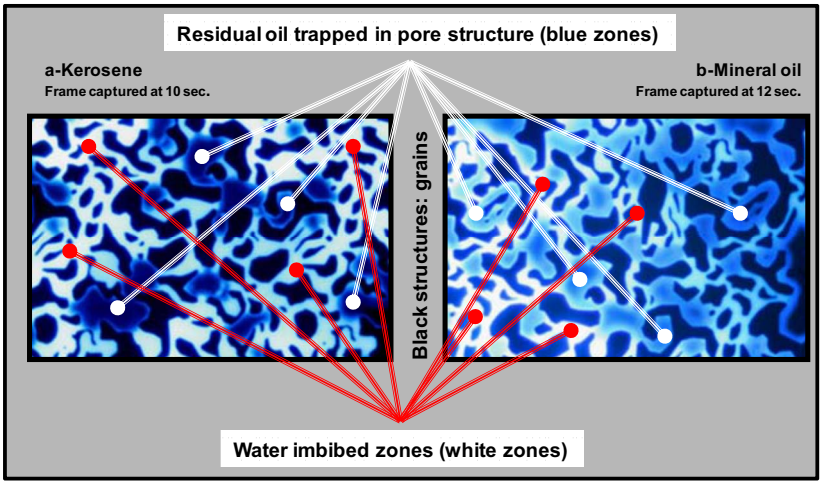

FIG. 13. (Color online) Residual oil saturation development for two different oil types. Water imbibes from left (white) displacing oil phase. The grains are in black color. Oil phase is in blue color (gray tones in the black and whit print). This experiment proves residual oil is directly related to pore structure. Image is 3000 μm wide.

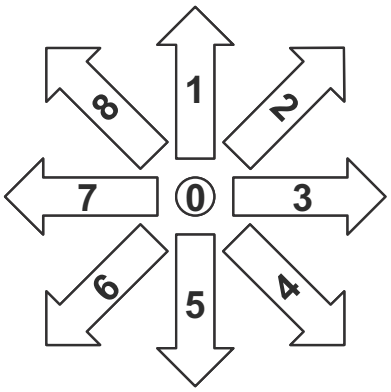

FIG. 14. Speed vectors used in the LBM simulations.

fluid cohesion (interfacial tension) as it was for miscible interaction. The additional forces, namely wettability (solid adhesion), IFT (fluid-fluid cohesion), and gravity were added to the velocity vector as follows to model immiscible interaction:

$$u = \frac{1}{\rho}\sum_i (R_i + B_i)^* c_i + F_g + F_c + F_a, \tag{4}$$

$$F_g = \rho_f g^* \Delta m, \tag{5}$$

where ρ_f denotes the occupation number for the carrier fluid (oil), g is gravity, and m is scaled mass, F_g forms to be the gravitational force. F_a (adhesion force) and F_c (cohesion force) are not equal to zero only when the neighbor is not the same as the occupied node. Simply the solid adhesion (F_a) is only applicable when the neighbor of the target cell is a solid node. Similarly, fluid-fluid cohesion (F_c) is nonzero when the neighbor node is occupied with the fluid of different type. The values of F_a and F_c are assigned empirically and would change as the viscosities (relaxation parameters) of the fluids change.

Because of the numerical constraints of the LBM, it is not possible to directly input the variables and therefore, scaling has to be applied. Assuming that IFT and wettability are viscosity dependent, fluid viscosities have to be scaled first.

Having in hand the real values of fluids and the model parameters, one can define (1) the viscosities of the fluid phases v [m/s^2], (2) the surface tension σ [N/m], (3) the strength of external force (gravity) g [m/s^2], (4) the densities of fluids ρ [kg/m^3], (5) the size of an LBM cell Δx [m] (resolution dependent). These parameters are used to set a reasonable time step size Δt [s] and limit the mass difference in the simulation Δm [kg]. The values of the LBM simulation are dimensionless and they should be converted to the dimensionless values as follows:

(1) lattice viscosity$=v^*(\Delta t/\Delta x^2)$, (2) lattice surface tension$=\sigma^*(\Delta t^2/\Delta m)$, (3) lattice force$=g^*(\Delta t^2/\Delta x)$, (4) lattice density$=\rho^*(\Delta x^3/\Delta m)$.

Here, the lattice density is used while calculating the external force (gravity). Occupation numbers for simulation of both phases are taken as unity. The value of Δt [s] will be used in matching the real experimental time values.

To define IFT and wettability, empirical constants F_a and F_c have to be calibrated for the desired fluids. To define these constants, virtual experiments were performed in different studies [26,41]. A commonly used method to define the fluid-cohesion parameter is to simulate varying sizes of droplets and check their compliance with the Laplace's law [18,42]. According to this, pressure difference within the droplet has to be larger than the surrounding fluid pressure.

Similarly solid adhesion F_a is defined using simulations. Both a droplet on a solid surface, and also virtual capillary tubes are used to calibrate the parameter as suggested by Christensen [26]. Since a strongly water wet media is desired, zero contact angle is assigned for F_a.

The parameters should be chosen within the algorithm constraints. According to the kinetic equation of lattice-gas automata (LGA), particles in one node with a velocity e_i after a time step Δt would be conserved unless any collision occurs. This is depicted with the Ω function, which is called the collision operator. As a derivative method of the LGA, the LBM incorporates the same equation which is

$$R_i(x + c_i, t + 1) = R_i(x,t) + \lambda_{vR} R_i^{neq}(x,t), \tag{6}$$

$$B_i(x + c_i, t + 1) = B_i(x,t) + \lambda_{vB} B_i^{neq}(x,t), \tag{7}$$

where R_i is red (water) and B_i is blue (oil) fluid densities. These two equations represent the particles at node(x,t) move with the unit speed c_i. Here $\lambda_{v\mathrm{R}}$ and $\lambda_{v\mathrm{B}}$ are the relaxation parameters which determine the kinematic viscosity v of each phase, respectively. The relationship between those parameters is given as

$$v_R = \frac{1}{3}\left(\lambda_{vR} - \frac{1}{2}\right), \tag{8}$$

$$v_B = \frac{1}{3}\left(\lambda_{vB} - \frac{1}{2}\right). \tag{9}$$

The fluid viscosity v is scaled, where this is used to calculate relaxation parameters ($\lambda_{v\mathrm{R}}$ and $\lambda_{v\mathrm{B}}$). The way relaxation parameter is defined [Eqs. (8) and (9)] puts restriction on the relaxation parameter, which is defined as $0.51 < \text{relaxation parameter} < 2.5$. Therefore, the scaling of the viscosity and definition of the lattice time scale were chosen accordingly.

Apart from the theoretical constraints, practical constraints also limit the range of viscosity. Our simulation runs showed that the interface between two phases becomes fuzzy for viscosity ratios four and higher. In an effort to make the interface sharper, the fluid-fluid cohesion (F_c) constant was increased and this caused instabilities at the run. Similar limitations of the method were also reported by different researchers [43,41].

B. Results

The LBM simulations were constructed to reflect the original experimental cases without much manipulation. For 5×5 cm original model dimension, 400 pixels were substituted to obtain a cell resolution of 0.125 mm which is the

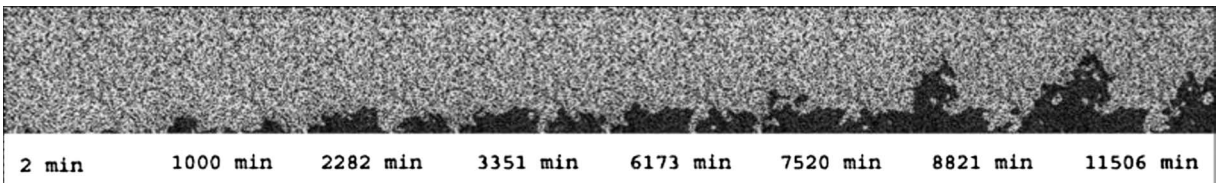

FIG. 15. Kerosene-water countercurrent imbibition simulation using the LBM (vertical orientation). Darker color represents the displacing-wetting-phase (water).

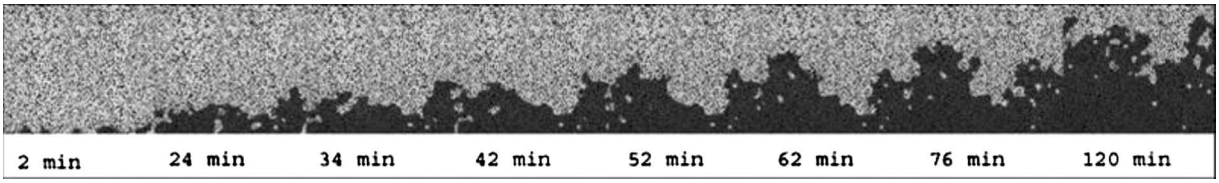

FIG. 16. Kerosene-water countercurrent imbibition simulation using the LBM (horizontal orientation). Darker color represents the displacing-wetting-phase (water).

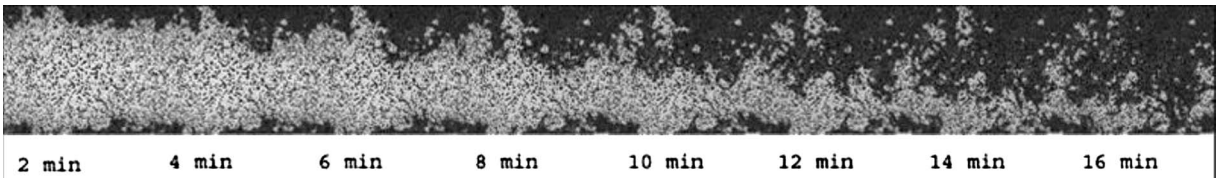

FIG. 17. Kerosene-water cocurrent imbibition simulation using the LBM (vertical orientation). Darker color represents the displacing-wetting-phase (water).

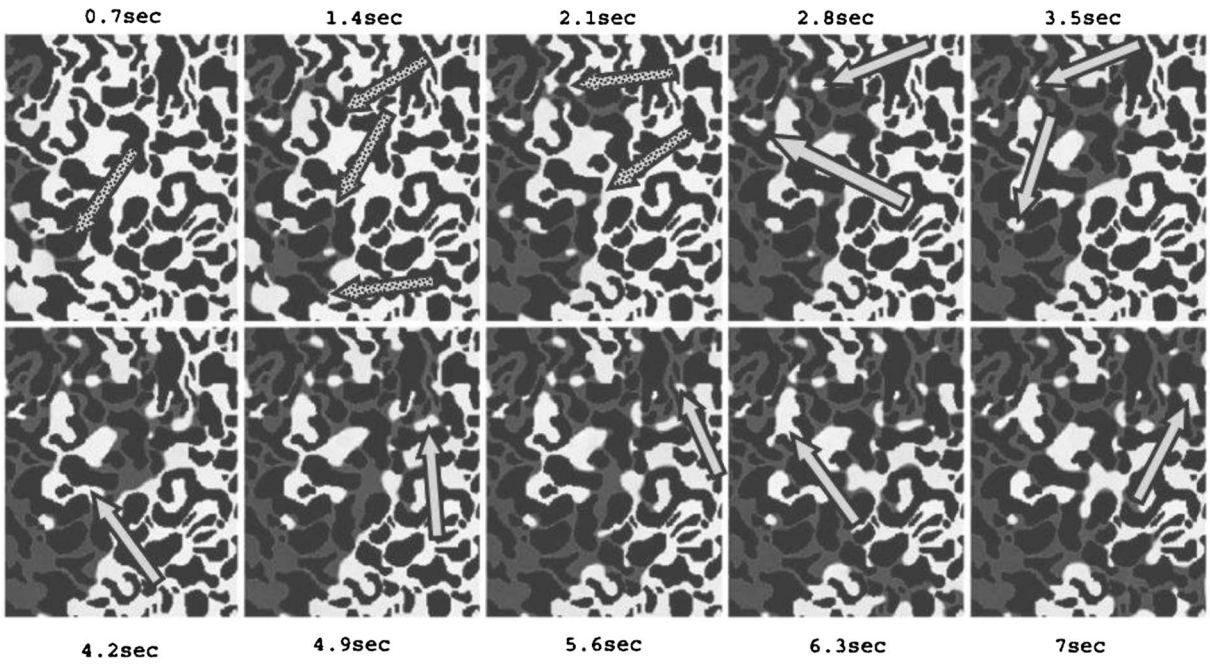

FIG. 18. Simulation results of spontaneous imbibition at microscale. Water imbibes from left (gray color) displacing oil (white color). The grains are in black color. Dotted arrows on the first three images indicate the invasion of the smallest size pores first. Solid arrows on the rest of the images point the residual saturation development. Displacement is controlled by countercurrent action even though the other end is open to flow. This portion covers a very small part of the model and the effect of the opposite boundary, which is open to flow, has not been felt yet. Therefore, the displacement occurs in countercurrent manner during the time period covered in this figure.

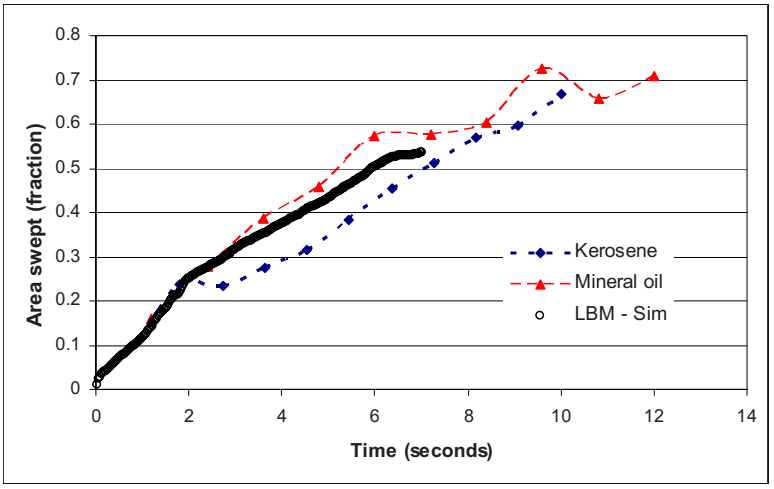

FIG. 19. (Color online) Area sweep performance curve for micromodel experiments and LBM simulation.

approximate size of a glass bead. Hence, theoretically, one pixel represents one pore (or grain) and the smallest pore space would be one node (or pixel). In practice this is not the case as the scattered grains allow pores to be much larger than four nodes. This is also in line with the real-life problem where it is almost impossible to pack the glass beads so densely and perfectly. The grains were assigned randomly and are very scattered to form pores smaller than four nodes linearly. It is a well known fact that four nodes of pore space are needed for the LBM to run properly, i.e., to recover the correct Navier-Stokes (NS) equation with nonslip boundary condition at the fluid and/or solid interface. In our case it is possible that this requirement may not be met at certain parts of the model depending on grain orientation (grains are assigned randomly and are very scattered). Our base was the glass-bead experiments that were performed for qualitatively and quantitatively match the LBM results. As we obtained satisfactory matches in both qualitative and quantitative terms, one can accept the grain and/or pore assignment in LBM simulations captures the physics accurately and the number of nodes used is an optimal value.

As mentioned above, the grains were assigned randomly and in this process, typically, 25% of 400×400 nodes were used as grains and the rest (75%) correspond to pores. This ratio was obtained through scanning the experimental (glass bead) models and setting a threshold value that distinguishes pores and grains. This is not a real measurement of porosity but totally based on the brightness value.

Different numbers of nodes were tested and obtaining a progressing front and a good match to the experimental images, we can confidently state that the 400×400 approximation would give results good enough to give ideas about the fluid progression. It is worthwhile noting that the larger grid sizes for this kind of simulation are not preferred because of computational constraints.

Boundary conditions were affiliated to reflect the experiment conditions; either 3 or 2 sides sealed. As the criterion to stop the simulation, the number of iterations was used. This depends on the type of the experiment and the experimental results were used to make a decision about the number of iterations.

The results of kerosene-water simulations are given in Fig. 15 for the countercurrent model of vertical orientation. Figure 16 displays the horizontal orientation. The gravity effect is apparently effective for the cocurrent model (Fig. 17). The simulation results show qualitatively similar trends for the progress of the displacement front even though the heterogeneity of the glass-bead models was thought to be a critical issue. The time matches for a quantitative analysis will be provided and discussed later in this section. The time match is not as high quality as for the cocurrent simulation compared to the countercurrent equivalent (Fig. 17). This is probably due to problems in the representation of the experimental model characteristics in exact manner on the LBM. Note that the gravity apparently controls the flow strongly on the top portion of the model as captured also captured well on the LBM simulation. But, the LBM simulations showed some small amount of intrusion from the bottom portion totally controlled by capillary forces and this was not observed in the experimental case.

The model was also tested at micromodel scale. The model pattern was digitized and the simulation was run on this image (Fig. 18). The displacement is controlled by countercurrent action even though the other end is open to flow. The portion of the micromodel shown in Figs. 11 and 12 and its LBM equivalent given in Fig. 18 covers a very small part of the model and we observed during the experimentation that the effect of the opposite boundary, which is open to flow, has not been felt yet. Therefore, the displacement occurred totally by capillary forces.

Comparing the two cases given in Figs. 11 and 18, one can observe that the development of residual phase saturation and the progress of the front are in a very similar fashion in both simulation and experiment. For the strongly water-wet medium the process is controlled by the pore structure (or pore scale heterogeneity). This can be seen in Fig. 11 by a rapid movement of the wetting phase in the smaller pores compared to bigger size pores. In other words, the process follows the general rule of capillarity, i.e., the smaller size pores are occupied first by the wetting phase. The same was captured in the simulation as marked by dotted arrows on the first three images of Fig. 18. Obviously, in case of less favorable wettability (mixed or intermediate wet) rather than strongly water-wet medium, the wettability will start playing a role on the dynamics of the process in addition to the pore size and heterogeneity.

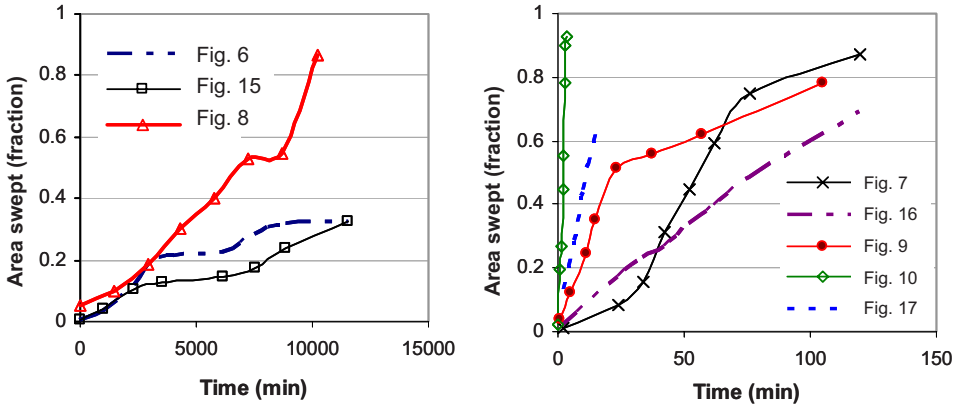

FIG. 20. (Color online) Area sweep performance curves for glass-bead experiments and corresponding LBM simulations.

Figures 19 and 20 are given to quantify the success of the match between experiments and simulations for the micromodel and glass bead models, respectively. For the LBM simulations, the unswept zones are clearly identifiable and therefore accurate area calculation was possible for the micromodel experiments (Fig. 19). The curves for mineral oil and kerosene show similar ultimate recovery values. The trend is captured for the simulation and a very close match is obtained with the respective kerosene experiment. Although the LBM simulation could not be performed for the mineral oil case due to limitations of the viscosity ratio, the curve showing the area swept for the mineral oil was included as a reference. The ultimate recovery value of the simulation falls slightly short because of the fact that the simulation had to be ceased before the imbibing phase reaches the end due to stability problems.

The same plots were provided for the glass-bead experiments (Fig. 20). For the images obtained from experimental studies, a threshold value had to be set to distinguish the oleic and aqueous phases. For this purpose, a threshold value was set and brighter pixels were regarded as unswept zones. As shown in Fig. 20, the kerosene experimental and LBM models yielded a good agreement for different displacement types, i.e., horizontal-vertical and countercurrent–cocurrent cases. As in the micromodel case, the results for the mineral oil were included in the plots as reference.

IV. CONCLUSIONS AND REMARKS

Two types of visual experimentation were provided to study matrix-fracture interaction by spontaneous (capillary) imbibition under static conditions, i.e., no flow in fracture. Glass-bead model experiments were performed as they provide changeable interaction types (countercurrent or cocurrent) by creating different model boundary conditions. This experimental scale also allowed capturing images using a camera without any high magnification requirement. Vertical and horizontal positioning was possible and this allowed us to observe the effect of gravity on the process. Silicon-etched micromodels were used for precise-pore-scale observation and clarifications on the dynamics of spontaneous imbibition (quasistatic displacement). High accuracy of the models also served as a testing platform for the proposed LBM model at the pore scale. The LBM model was not only able to successfully capture the scaling in terms of viscosity and time, it also was able to simulate the effect of gravity on a larger scale, as tested on the glass-bead models.

Remarkable amount of research has been published previously on the theory of the LBM, where the amount of experimental work to test the model was less in number. The method is especially strong to model flow within porous media, since the fluid velocity effects are minimal. For this study, solely spontaneous imbibition was the driving mechanism, where wettability of the porous media defines the interaction dynamics. The model was not given specific orders to dictate the direction of flow. The process occurred as the wettability of the rock surfaces causes the wetting phase to move and displace the nonwetting phase within the matrix. Pore size and heterogeneity and overall matrix geometry play a very important role as confirmed by experimental findings. The LBM was able to capture the physical mechanism, and was accurate enough to display a similar residual oil saturation patterns as in the experimental case performed on the micromodel. The same model was applied to glass-bead experiments in an effort to model kerosene-water interaction. Similar fingering behavior, the effect of gravity, and lattice-time–real-time conversion were successfully captured. The previous finding on application limits of the LBM technique for immiscible displacement, i.e., the maximum allowable viscosity ratio is four, was also verified.

ACKNOWLEDGMENTS

This study was partly funded by two NSERC Grants (No. G121210595 and Strategic Grant No. G121990070). The funds for the equipment used in the experiments were obtained from the Canadian Foundation for Innovation (CFI) (Project No. 7566) and the University of Alberta. We gratefully acknowledge this support.

[1] C. C. Mattax and J. R. Kyte, SPEJ **2**, 177 (1962).
[2] B. J. Bourbiaux and F. J. Kalaydjian, in the *Proceedings of the SPE Annual Technology Conference and Exhibition*, Houston, Texas, 1988 (unpublished), SPE 18283.
[3] X. Zhang, N. R. Morrow, and S. Ma, SPE Reservoir Eng. **11**, 280 (1996).
[4] A. Kantzas, M. Pow, K. Allsopp, and D. Marenette, *Proceedings of the 7th Petroleum Society of CIM Petroleum Conference of the South Saskatchewan Section*, 1997 (unpublished), paper 97–181.
[5] E. Rangel-German and A. R. Kovscek, in the *Proceedings of the SPE Annual Techonology Conference and Exhibition*, Denver, Colorado, 2003 (unpublished), SPE 84411.
[6] F. Civan and M. L. Rasmussen, in *Proceedings of the SPE Production and Operation Symposium*, Oklahoma City, Oklahoma, 2005 (unpublished), SPE 94267.
[7] T. Babadagli, J. Colloid Interface Sci. **156**, 203 (2002).
[8] T. Babadagli, SPEJ **6**, 465 (2001).
[9] C. U. Hatiboglu and T. Babadagli, J. Pet. Sci. Eng. **59**, 106 (2007).
[10] C. U. Hatiboglu and T. Babadagli (unpublished).
[11] D. S. George and A. R. Kovscek, Stanford University, Technical Report, USA, 2001 (unpublished).
[12] N. S. Sagar and L. M. Castanier, Stanford University, Technical Report, 1997 (unpublished).
[13] U. Frisch, B. Hasslacher, and Y. Pomeau, Phys. Rev. Lett. **56**, 1505 (1986).
[14] L. Kadanoff, Phys. Today **39**, 7 (1986).
[15] R. Benzi, S. Succi, and M. Vergassola, Phys. Rep. **222**, 145 (1992).
[16] D. H. Rothman and S. Zaleski, Rev. Mod. Phys. **66**, 1417 (1994).
[17] S. Chen and G. D. Doolen, Annu. Rev. Fluid Mech. **30**, 329 (1998).
[18] X. Shan and H. Chen, Phys. Rev. E **47**, 1815 (1993).
[19] C. U. Hatiboglu and T. Babadagli, Phys. Rev. E **76**, 066309 (2007).
[20] Michael R. Swift, W. R. Osborn, and J. M. Yeomans, Phys. Rev. Lett. **75**, 830 (1995).
[21] G. Hazi, A. T. Imre, G. Mayer, and I. Farkas, Ann. Nucl. Energy **29**, 1421 (2002).
[22] R. R. Nourgaliev, T. N. Dinh, T. G. Theofanous, and D. Joseph, Int. J. Multiphase Flow **29**, 117 (2003).
[23] M. C. Sukop and D. Or, Water Resour. Res. **40**, w01509 (2004).
[24] P. Raiskinmaki, A. Shakib-Manesh, A. Jasberg, A. Koponen, J. Merikoski, and J. Timonen, J. Stat. Phys. **107**, 143 (2002).
[25] X. Zhang, A. G. Bengough, L. K. Deeks, J. W. Crawford, and I. M. Young, Water Resour. Res. **38**, 1167 (2002).
[26] B. S. B. Christensen, Ph.D. thesis, Institute of Environment & Resources Technical University of Denmark, 2006.
[27] J. W. Hornbrook, L. M. Castanier, and P. Pettit, Stanford University Report No. SUPRI TR-86, 1992 (unpublished).
[28] F. Woody, M. Blunt, and L. M. Castanier, Stanford University Report No. SUPRI TR-100, 1995 (unpublished).
[29] T. O. Lolomari, M.S. thesis, Stanford University, 1996.
[30] F. A. L. Dullien, *Porous Media: Fluid Transport and Pore Structure* (Academic, San Diego, CA, 1992).
[31] Y. H. Qian, D. D'Humieres, and P. Lallemand, Europhys. Lett. **17**, 479–484 (1992).
[32] H. Chen, S. Chen, and W. Matthaeus, Phys. Rev. A **45**, R5339 (1992).
[33] A. K. Gunstensen, D. H. Rothman, S. Zaleski, and G. Zanetti, Phys. Rev. A **43**, 4320 (1991).
[34] D. H. Rothman and J. M. Keller, J. Stat. Phys. **52**(3/4), 1119 (1988).
[35] H. W. Stockman, R. J. Glass, C. A. Cooper, and H. Rajaram, Int. J. Mod. Phys. C **9**, 1545 (1998).
[36] A. Cali, S. Succi, A. Cancelliere, R. Benzi, and M. Gramignani, Phys. Rev. A **45**, 5771 (1992).
[37] E. G. Flekkoy, Phys. Rev. E **47**, 4247 (1993).
[38] N. S. Martys and H. Chen, Phys. Rev. E **53**, 743 (1996).
[39] S. Chen, S. P. Dawson, G. D. Doolen, D. R. Janecky, and A. Lawniczak, Comput. Chem. Eng. **19**, 617 (1996).
[40] I. W. Yeo and S. Ge, Geophys. Res. Lett. **28**, 3983 (2001).
[41] J. Chin, E. S. Boek, and P. V. Coveney, Proc. R. Soc. London, Ser. A **360**, 547 (2002).
[42] C. Pan, M. Hilbert, and C. T. Miller, Water Resour. Res. **40**, W01501 (2004).
[43] N. Thurey, M.S. thesis, Friedrich-Alexander-Universitat Erlangen-Nurnberg, 2005.